⌘ *Author's Choice*

THE JOURNAL OF BIOLOGICAL CHEMISTRY VOL. 287, NO. 50, pp. 42104–42118, December 7, 2012

Reengineering the Collision Coupling and Diffusion Mode of the A_{2A}-adenosine Receptor

PALMITOYLATION IN HELIX 8 RELIEVES CONFINEMENT[*S]

Received for publication, June 19, 2012, and in revised form, October 10, 2012 Published, JBC Papers in Press, October 15, 2012, DOI 10.1074/jbc.M112.393579

Simon Keuerleber[1], **Patrick Thurner**[1], **Christian W. Gruber, Jürgen Zezula, and Michael Freissmuth**[2]

From the Institute of Pharmacology, Center of Physiology and Pharmacology, Medical University of Vienna, Währinger Strasse 13A, 1090 Vienna, Austria

Background: The A_{2A} receptor engages G_s by restricted collision coupling and lacks a palmitoyl moiety in its C terminus.
Results: Engineering palmitoylated cysteine into the C terminus relieved restricted collision coupling and resulted in accelerated diffusion of the agonist-liganded A_{2A} receptor.
Conclusion: Restricted collision coupling arises from limits imposed on receptor diffusion.
Significance: Agonist induced confinement of the A_{2A} receptor in a structure consistent with a lipid raft.

The A_{2A}-adenosine receptor undergoes restricted collision coupling with its cognate G protein G_s and lacks a palmitoylation site at the end of helix 8 in its intracellular C terminus. We explored the hypothesis that there was a causal link between the absence of a palmitoyl moiety and restricted collision coupling by introducing a palmitoylation site. The resulting mutant A_{2A}-R309C receptor underwent palmitoylation as verified by both mass spectrometry and metabolic labeling. In contrast to the wild type A_{2A} receptor, the concentration-response curve for agonist-induced cAMP accumulation was shifted to the left with increasing expression levels of A_{2A}-R309C receptor, an observation consistent with collision coupling. Single particle tracking of quantum dot-labeled receptors confirmed that wild type and mutant A_{2A} receptor differed in diffusivity and diffusion mode; agonist activation resulted in a decline in mean square displacement of both receptors, but the drop was substantially more pronounced for the wild type receptor. In addition, in the agonist-bound state, the wild type receptor was frequently subject to confinement events (estimated radius 110 nm). These were rarely seen with the palmitoylated A_{2A}-R309C receptor, the preferred diffusion mode of which was a random walk in both the basal and the agonist-activated state. Taken together, the observations link restricted collision coupling to diffusion limits imposed by the absence of a palmitoyl moiety in the C terminus of the A_{2A} receptor. The experiments allowed for visualizing local confinement of an agonist-activated G protein-coupled receptor in an area consistent with the dimensions of a lipid raft.

The A_{2A}-adenosine receptor is of interest for several reasons. (i) It is among the most frequently blocked pharmacological targets because it is the site of action of caffeine (1). In fact, in prospective studies blockage of the A_{2A} receptor by caffeine consumption reduces the risk of developing Parkinson disease (2). Accordingly, the A_{2A}-selective antagonist istradefylline has entered phase III clinical trials (3, 4). The efficacy of istradefylline is remarkable because it is first non-dopaminergic compound shown to be active in Parkinson disease. Conversely, topical preparations of A_{2A}-selective agonists are tested in clinical trials, *e.g.* for promotion of dermal wound healing and for suppression of asthma (5, 6), the underlying rationale being the observation that A_{2A} receptor activation stimulates endothelial cell proliferation (7, 8) and suppresses proinflammatory signals in macrophages and T-cells (9), respectively. (ii) When compared with other G protein-coupled receptors (GPCRs)[3] of the class A (rhodopsin-like) GPCRs, the A_{2A} receptor has a long C terminus that provides a docking site for several proteins that directs the fate of the receptor from its site of synthesis in the endoplasmic reticulum to its lysosomal degradation (10). In addition, the long C terminus also allows for recruitment of additional signaling molecules (11, 12). (iii) The structure of the A_{2A} receptor is understood at atomic resolution in both the antagonist- (13) and the agonist-bound state (14, 15). Structure-based molecular dynamics simulations suggest that the A_{2A} receptor may have a cholesterol binding site that promotes agonist binding; this may allow the receptor to sample the membrane environment (16). In fact, cholesterol depletion precludes coupling of the receptor to G_s but does not impede its ability to recruit ARNO and to activate ERK phosphorylation (17). (iv) The vast majority of GPCRs carry one or several cys-

* This work was supported by the Ph.D. Program "Cell Communication in Health and Disease" funded jointly by the Medical University of Vienna and the Austrian Science Fund/Fonds zur Förderung der wissenschaftlichen Forschung (FWF), Grants P20012 and PIRG-GA-2008-230970 from the Austrian Science Fund/FWF, and the European Union-funded Marie Curie training and mobility program.
⌘ *Author's Choice*—Final version full access.
[S] This article contains supplemental Table S1, Fig. S1, and Videos 1 and 2.
[1] Both authors contributed equally.
[2] To whom correspondence should be addressed. Tel.: 43-1-4277-64171; Fax: 43-1-4277-9641; E-mail: michael.freissmuth@meduniwien.ac.at.

[3] The abbreviations used are: GPCR, G protein-coupled receptor; ARNO, ADP-ribosylation factor nucleotide-binding site opener (a guanine nucleotide exchange factor for ARF6); CGS21680, 3-[4-[2-[[6-amino-9-[(2*R*,3*R*,4*S*,5*S*)-5-(ethylcarbamoyl)-3,4-dihydroxy-oxolan-2-yl]purin-2-yl]amino]ethyl]phenyl]propanoic acid; ERK1/2, extracellular signal-regulated kinase-1 and -2 = MAPK, p44/p42 mitogen-activated protein kinase; FRAP, fluorescence recovery after photobleaching; MRM, multiple reaction monitoring; MSD, mean square displacement; ZM241385, 4-(2-[7-amino-2-(2-furyl)-[1,2,4]-triazolo-[2,3-a]-[1,3,5]-triazin-5-ylamino]ethyl)phenol); GTPγS, guanosine 5′-*O*-(thiotriphosphate).

teine residues in their C terminus some 20 amino acids removed from the end of transmembrane helix 7. The cysteine residue(s) is subject to palmitoylation. This modification is thought to anchor the amphipathic helix 8, which runs parallel to the membrane plane, and stabilize it (18). In the A_{2A} receptor there is not any cysteine in this region. This is also true for the chemokine receptor CXCR4 (the receptor for stromal cell-derived factor/CXCL12). In contrast to CXCR4, in which helix 8 only comprises a single turn followed by an extended flexible segment (19), helix 8 in the A_{2A} receptor has four helical turns, and this is seen in both the antagonist- and the agonist-bound state (13–15). It is, therefore, not clear why the A_{2A} receptor should have evolved to lack the palmitoylation site. (iv) The A_{2A} receptor has long been known to differ from other G_s-coupled receptors by its G protein-coupling mode (20); when examined in the same cell (*i.e.* the turkey erythrocyte membrane), the β-adrenergic receptor has access to all G_s moieties, whereas the A_{2A} receptor can only promote activation of a limited number of available G_s molecules. This coupling mode was termed "restricted collision coupling" (20, 21). Restricted collision coupling is not a unique property of the turkey erythrocyte membrane. It can also be observed in mammalian cells, where the A_{2A} receptor is expressed endogenously, *e.g.* the human platelet (22).

In the present work we explored the hypothesis that there is a link between restricted collision coupling and the absence of a palmitoyl moiety in the C terminus of the A_{2A} receptor because its absence limited the membrane area that was visited by the agonist-activated A_{2A} receptor. In fact, engineering a palmitoylation site into the A_{2A} receptor eliminated restricted collision coupling, accelerated diffusion of the quantum dot-labeled receptor and eliminated its confinement that was seen in the agonist-bound state.

EXPERIMENTAL PROCEDURES

Materials—All cell culture reagents and Lipofectamine Plus™ were from Invitrogen except fetal calf serum (FCS; PAA Laboratories; Pasching, Austria). [2,8-^{3}H]Adenine (28.1 Ci/mmol) and [9,10-^{3}H(N)]palmitic acid (47.7 Ci/mmol) were purchased from PerkinElmer Life Sciences, [^{3}H]ZM241385 (specific activity, 50 Ci/mmol) was from American Radiolabeled Chemicals, Inc. (St. Louis, MO), unlabeled ZM241385 was from Tocris Bioscience (Bristol, UK), quantum dots Q11022MP Qdot® 655 goat F(ab′)2 anti-mouse IgG conjugate (H+L) was from Molecular Probes/Invitrogen, and mouse monoclonal anti-FLAG® M2 antibody and casein from bovine milk were from Sigma. Polyclonal antibodies recognizing ERK1/2 (p44/42 MAP kinase) and its dual-phosphorylated (active) form were purchased from Cell Signaling Technology (Danvers, MA), the mouse monoclonal antibody against the A_{2A}-adenosine receptor (clone 7F6-G6-A2) was from Millipore (Billerica, MA), the rabbit polyclonal antibody against flotillin-1 was from Sigma, the rabbit polyclonal antibody (ab290) against GFP was from Abcam Plc (Cambridge, UK), the rabbit antiserum directed against Gβ was raised against amino acids 8–23 of G$\beta_{1/2}$ (23), and protein A-Sepharose, anti-mouse and anti-rabbit IgG1 (HRP) horseradish were from GE Healthcare. Complete protease inhibitor mixture was from Roche Applied Science. The source of the other reagents and chemicals has been listed previously (17).

Cell Transfection and Cell Culture—Arginine 309 was replaced by cysteine in the human A_{2A} receptor cDNA using the QuikChange Lightning site-directed mutagenesis kit (Stratagene, Carlsbad, CA). The forward primer sequence of the forward primer sequence was as follows (5′ to 3′ direction with the mutated nucleotides indicated in bold and underlined to introduce the R309C mutation and a silent mutation for insertion of an Eco72I/PmaCI site, respectively): C ATT CGC AGC CAC GT**G** CTG TGC CAG CAA GAA CCT TTC. Several versions of the receptor cDNA were prepared, namely one encoding wild type and mutant receptors tagged on their C terminus with YFP. The sequence was confirmed by automated DNA sequencing. Human embryonic kidney (HEK) 293 cells were maintained in Dulbecco's modified Eagle's medium (DMEM) containing high glucose (4.5 g/liter = 25 mM), 10% FCS, and 2 mM glutamine at 37 °C in a 5% CO_2 humidified atmosphere. For transient expression, HEK293 cells were transfected with plasmids encoding wild type or mutant A_{2A} receptor using the calcium phosphate precipitation method. These cells were used 24–48 h later for experiments. For the generation of stable cells lines, transfected cells were subjected to selection in the presence of Geneticin (G418; 0.5 to 0.75 g/liter). After 7–14 days single colonies emerged that were expanded and maintained in the presence of 0.25 g/liter G418. In some instances HEK293 cells expressing an YFP-tagged A_1 receptor (24) were used as a control. Receptor expression was visualized by confocal microscopy on a Zeiss Axiovert 200-LSM 510 microscope equipped with argon and helium/neon lasers (30 and 1 milliwatt, respectively) and a 63× oil immersion objective (Zeiss Plan-Neofluar) as in Ref. 17. Stable HEK293 cell lines expressing FLAG-tagged wild type A_{2A} receptor and A_{2A}-R309C receptor were produced by retroviral infection using pBABE-puro. The retroviruses were produced in Phoenix ecotropic cells. Infected cells were subjected to selection with puromycin (2 μg/ml).

Cyclic AMP Accumulation, Radioligand Binding, and ERK Phosphorylation—The conditions for determining agonist-stimulated cAMP accumulation are outlined in Ref. 25. In brief, cells (3^*10^5/well) were seeded into poly-D-lysine-coated 6-well culture plates. On the following day the cellular ATP pool was metabolically labeled by incubating cells for 16 h with [^{3}H]adenine (1 μCi/well). Cells were starved by removing FCS from the culture medium, and the cells were subsequently incubated for 1 h in the presence of the phosphodiesterase inhibitor Ro-20–1724 (100 μM) and adenosine deaminase (5 μg/ml). The formation of cAMP was stimulated by the addition of different concentrations of CGS21680 for 20 min at 37 °C. Agonist-stimulated ERK phosphorylation was assessed as in Ref. 26. Samples of cellular lysate (20–30 μg of protein) were electrophoretically resolved and transferred to a nitrocellulose membrane. Activation of MAPK was detected using an anti-phospho-ERK1/2 antibody; anti-holo-ERK1/2 antibody served as the loading control. Immunoreactive bands were visualized using a FluorChemHD2 imaging system (Alpha Innotech Corp., San Leandro, CA) and quantified using ImageJ (Version 1.45r). Binding assays were carried out with the high affinity A_{2A}-se-

lective antagonist [^{3}H]ZM241385 in a final volume of 0.2 ml containing 50 mM Tris·HCl, pH 7.5, 5 mM $MgCl_2$, 1 mM EDTA, 5 μg/ml adenosine deaminase, and additional reagents as outlined in the figure legends. Reaction conditions were as described in Ref. 17 except that membranes were used instead of intact cells. These membranes were prepared by resuspending HEK293 cells stably expressing wild type and mutated receptors in buffer containing 25 mM HEPES·NaOH, pH 7.5, 2 mM $MgCl_2$, 1 mM EDTA and subjecting the suspension to two freeze-thaw cycles followed by sonication (4 times for 10 s in an ice-cold water bath). Membranes were harvested by centrifugation at 34,000 $\times$ *g* for 30 min. The pellet was resuspended in the buffer described above. The protein concentration was estimated by Coomassie Blue binding and adjusted in the binding reaction (5–100 μg/assay) to avoid radioligand depletion.

Metabolic Labeling with [^{3}H]Palmitate and Immunoprecipitation—Labeling was done as described by (27) with the following modifications; cells (3×10^5/well) were seeded into 6-well plates and allowed to adhere. After 20 h, the cells were lipofected with plasmids encoding FLAG-tagged versions of wild type A_{2A} receptor, A_1 receptor, or A_{2A}-R309C receptor. After 4 h, the medium was replaced, and cells were grown for another 24 h. Cells were preincubated in serum-free medium supplemented with 10 mg/ml fatty acid-free bovine serum albumin, then labeled with [^{3}H]palmitate (0.25 mCi/well) for 4 h, washed with phosphate-buffered saline, and resuspended in 0.15 ml buffer (20 mM Tris-HCl, pH 7.4, 1 mM EDTA, 100 mM NaCl, 1% SDS). After 5 min, Triton X-100-containing buffer (20 mM Tris-HCl pH 7.4, 1 mM EDTA, 100 mM NaCl, 1% Triton X-100) was added to dilute the SDS concentration to 0.1%. The sample was centrifuged at 16,000 $\times$ *g* for 10 min, and the resulting supernatant was incubated overnight with anti-GFP antibody (2 μl corresponding to 10 μg of total IgG) under gentle rotation at 4 °C. Subsequently, pre-equilibrated protein A-Sepharose (6 mg per sample) was added and incubated with gentle rotation at 4 °C for 3 h. Samples were washed three times with Triton X-100-containing lysis buffer and eluted by heating the samples in 0.1 ml loading buffer (62.5 mM Tris-HCl, pH 6.8, 10% glycerol, 2% SDS, 0.001% bromphenol blue) at 95 °C for 2 min. An aliquot of the sample (40 μl) was analyzed by SDS-PAGE, the gel was fixed for 30 min in fixing solution (isopropyl alcohol: water:acetic acid = 25:65:10) incubated in NAMP100 (GE Healthcare) for 30 min, dried, and then exposed to x-ray film (Kodak BioMax MS) at −80 °C for 2–8 weeks.

Nano-LC-MS/MS and Multiple Reaction Monitoring (MRM) Mass Spectrometry—Membranes were prepared from cells expressing FLAG-tagged versions of wild type A_{2A} receptor and A_{2A}-R309C receptor as outlined above. Membranes (1 mg/ml) were solubilized in buffer containing 25 mM HEPES·NaOH, pH 7.5, and 0.2 mM dodecyl-β-maltoside. The unsolubilized material was removed by ultracentrifugation (250,000 $\times$ *g* for 2 h at 4 °C), and the resulting supernatant was incubated with pre-equilibrated anti-FLAG M2-agarose beads for 1 h at 4 °C. Beads were transferred to a gravity flow column and washed 3 times with 0.5 ml of solubilization buffer containing 1% Triton X-100. The column was incubated twice with 0.1 ml buffer containing Tris-HCl (20 mM, pH 8) and 6 M urea buffer for 10 min at 25 °C under stopped-flow conditions. The eluate was collected by spinning the column in a tabletop centrifuge (30 $\times$ *g* for 1 min). The eluate was transferred to a Microcon Ultracel YM-3 column (Millipore GmbH) and concentrated by centrifugation. The desalted and concentrated sample was digested with trypsin for 12–16 h at 37 °C. Concentrated acetic acid was added to stop the digestion reaction. Digested samples were analyzed by nano-LC-MS/MS using information-dependent acquisition for mapping of tryptic A_{2A} receptor peptides and MRM mass spectrometry to identify the palmitoylated peptide. A Dionex Ultimate 3000 nano-HPLC system (Dionex, Amsterdam, The Netherlands) in pre-concentration mode was used for reversed phase separation of the samples before MS using a Dionex Acclaim PepMap 100 C_{18} 100 Å column (150 mm $\times$ 75 μm) with a particle size of 3 μm. The mobile phase consisted of solvent A (0.1% aqueous formic acid) and solvent B (80/20 acetonitrile/0.08% aqueous formic acid). Tryptic peptides were eluted using a gradient of 4–60% solvent B in 40 min at a flow rate of 300 nl/min. The eluate was directly introduced into a hybrid triple quadrupole/linear ion trap 4000 QTRAP MS/MS system (AB Sciex) equipped with a NanoSprayII ion source and was operated with Analyst 1.5.2 software. The experiments were performed in positive ionization mode. Nebulizer gas, ion spray voltage, and declustering potential were optimized for each experiment. Information-dependent acquisition experiments for tryptic peptide identification of the receptor included enhanced MS to examine the molecular weight of peptide ions and enhanced resolution scans to confirm charge states of the ions. Detection of ions above threshold with a charge state of +2 to +5 or with an unknown charge state triggered collision-induced dissociation of three enhanced product ion scans to collate fragment ions and present the product ion spectrum for subsequent database searches. Database searching was carried out using the ProteinPilot™ software (Version 4.0) and the Paragon algorithm (AB Sciex). MRM acquisition was performed with a dwell time of 50 ms and Q1/Q3 set in unit resolution. At least three Q1/Q3 transitions were monitored for each tryptic peptide (see supplemental Table S1). The MRM transitions were identified experimentally from the nano-LC-MS/MS information-dependent acquisition experiments; the transition of the *S*-palmitoylated peptide was calculated by adding the net mass of 238 Da.

Preparation of Detergent-resistant Membrane Fractions—HEK293 cells stably expressing wild type A_{2A} receptor or A_{2A}-R309C receptor were grown in 150-mm culture dishes. Two dishes were used for each experiment. Membranes were subjected to density gradient centrifugation as described (28) with the following modifications. Confluent cells were incubated in DMEM without FCS for 30 min followed by the addition of 3 μM CGS 21680 for a further 30 min. Membranes were prepared as described above, resuspended in 0.5 ml of buffer (50 mM Tris, pH 7.4, 2 mM EDTA, 150 mM NaCl), and homogenized by 10 aspiration cycles each through a 20- and a 27-gauge needle. Buffer (0.5 ml) containing 0.5% Triton X-100 was added. Extraction was done on ice for 30 min. The lysate (0.7 ml) was adjusted to 42% (wt/wt) sucrose by adding 1.4 ml of 59% sucrose in buffer, overlaid with 6 ml of 35% and 4 ml of 5% sucrose, and centrifuged at 217,000 $\times$ *g* for 18 h. Samples were fractionated in 1-ml aliquots from the top (fraction 1) to the bottom.

Single Particle Tracking—Cells (2×10^4/well) were seeded onto PDL poly-D-lysine-coated glass coverslips (diameter 25 mm) in 6-well culture dishes and maintained in medium (DMEM containing 25 mM glucose and 10% FCS) overnight at 37 °C and 5% CO_2. A master mix was prepared containing 3% casein (for blockage of nonspecific binding sites), a 1:1 ratio of quantum dots (0.5 μM final) reagent, and anti-FLAG antibody (0.5 μg/μl final) in Krebs-HEPES buffer (10 mM HEPES·NaOH, pH 7.5, 120 mM NaCl, 3 mM KCl, 2 mM $MgCl_2$, 2 mM $CaCl_2$, 22 mM glucose) and incubated for 15 min at 22 °C. This was diluted to concentrations that allowed for binding of only a few quantum dots per cell (usually in the range of $1:10^5$). Coverslips were removed from the 6-well plate, washed repeatedly in 37 °C PBS, placed in a humid chamber on a heating plate, and incubated with the diluted suspension of FLAG antibody-coated quantum dots for 20 min. After several washing steps, the coverslips were placed in a microscopy chamber and immersed in 1 ml of Krebs-HEPES buffer containing 5 μg/ml adenosine deaminase in the absence (basal state recordings) and presence of 10 μM CGS21680 (agonist activation).

Stacks were recorded in Visiview1.7.0 (Visitron Systems) on a Carl Zeiss Axiovert 135M inverted epifluorescence microscope (Zeiss Objective Alpha Plan-Apochromat 100×/1.46, Chroma 33012 QDOT655 filter set) with a cascade II:512 (maximum full frame acquisition time of 36 ms, 16 μm × 16 μm/pixel resulting in an actual pixel dimension of 0.16 μm × 0.16 μm) EMCCD camera (gain 3900 arbitrary units). Window size was adjusted to allow for faster acquisition and for obtaining tracks of 1000 frames at 50 frames/s with a pointing accuracy of 10–25 nm. After recording, bright field illumination was used to confirm the location of the quantum dot on the cell and to discard spurious trajectories. The minimum length of a reconnected trajectory was 100 frames, blinking events of up to 30 frames were allowed, and trajectories containing the merging of two or more quantum dots were dismissed.

Stack files and bright field images were transferred to and analyzed in MATLAB® VersionR2009a (The MathWorks™) with an adapted version of the tracklight software kindly provided by Daniel Choquet (University of Bordeaux, France). Analysis was done as described (29). In brief, the region-based segmentation algorithm for detection was supplemented by a maximum likelihood estimation of a two-dimensional Gaussian mask, which accounts for the Poisson distribution of the photon count per pixel (30). In addition, to allow for tracking of multiple particles, track.m-file was used for connection of trajectories (Daniel Blair and Eric Dufresne, The Matlab Particle Tracking Code Repository). At every step, a visual output was generated to verify the location of the imaged quantum dot and the connected trajectories. Mean squared displacement was calculated for each trajectory using Equation 1 (31),

$$\mathrm{MSD}(n\delta t) = 1/(N\text{-}1\text{-}n)\sum[x(j\delta t + n\delta t) - x(j\delta t)]^2 \; [y(j\delta t + n\delta t) - y(j\delta t)]^2 \quad \text{(Eq. 1)}$$

Diffusion coefficients (D_{1-4}) were estimated from a linear regression of the initial values of the mean square displacement (MSD) curve to the affine function (Equation 2) (32),

$$\mathrm{MSD}_{\mathrm{initial}}(\Delta t) - 4 \times \mathrm{D}_{\mathrm{initial}} \times \Delta t + 2\sigma^2 \quad \text{(Eq. 2)}$$

The diffusion mode of the individual trajectories. *i.e.* random walk, transported, or confined, was examined and analyzed as follows. Confined diffusion was separated from random walk by a predefined threshold; the pooled and averaged macroscopic diffusion coefficient (D_{mac}, obtained from fitting the first quarter of the MSD curve to the above equation) was calculated for each condition (basal, agonist-treated) and multiplied by (the one-tailed α-value of) 0.05 to define candidate outliers. Trajectories falling below this threshold were then fitted with MATLAB nonlinear least square regression employing the Trust-Region method to the equation for circular shaped domains (Equation 3) (33),

$$\mathrm{MSD}_t = \mathrm{AREA} \times [1 - \mathrm{F}_1 \times e^{(-4 \times \mathrm{F2} \times \mathrm{D1} - 4 \times \mathrm{t/AREA})}] \quad \text{(Eq. 3)}$$

Briefly, this represents the expansion of the first two terms from the exact series solution for circular corrals (Equation B14 in the appendix to Ref. 34), where the factors F_1 and F_2 are calculated (from the roots of Bessel function derivatives), whereas the AREA is estimated from the fit. The resulting apparent confinement radius ($\rho_{\mathrm{app}} = \sqrt{\mathrm{AREA}/\pi}$) was included for correlations with R^2 greater than 0.75 and a D_{mac}/D_{1-4} ratio <0.5, whereas all other potential confinements were discarded (because the stochastic diffusion process may mimic confinement).

Statistics—Concentration-response curves, saturation curves, and radioligand displacement curves were subjected to non-linear least squares curve-fitting to equations describing a rectangular hyperbola, the sum of two hyperbolas, or the Hill equation using a Marquardt-Levenberg algorithm. The improved fit associated with the choice of the more complex model was evaluated by an F-test based on the extra sum-of-squares principle. Diffusion coefficients were rounded to 10^{-3} $\mu m^2/s$ and logarithmically transformed for further analysis. The cumulative frequency distributions of diffusivity (depicted as empirical cumulative distribution functions) were analyzed using Kolmogorov-Smirnov test for two empirical distributions. The Kruskal-Wallis test followed by Dunn's multiple comparisons were used to compare diffusivity of all four groups.

RESULTS

Introducing a Putative Palmitoylation Site Does Not Affect Cell Surface Expression and Ligand Binding of the A_{2A} Receptor—The vast majority of group I (rhodopsin-like) G protein-coupled receptors carries one (or two) palmitoylated cysteine(s) within the proximal portion of their C terminus (typically some 20 residues away from the end of the seventh transmembrane segment (TM7)). Strikingly, the A_{2A} receptor does not have any cysteine residue in the proximal segment. Moreover, there is only a single cysteine in position 394 in the human receptor that is absent in other species, *e.g.* mouse or rat. Finally, it was shown that the human A_1 receptor carries a palmitate thioester at a cysteine corresponding to position 309 of the A_{2A} receptor (35). This cysteine is conserved in the human A_{2B} and A_3 receptors (Fig. 1*A*). We, therefore, substituted the arginine 309 with cysteine and tested if this renders the mutated receptor sus-

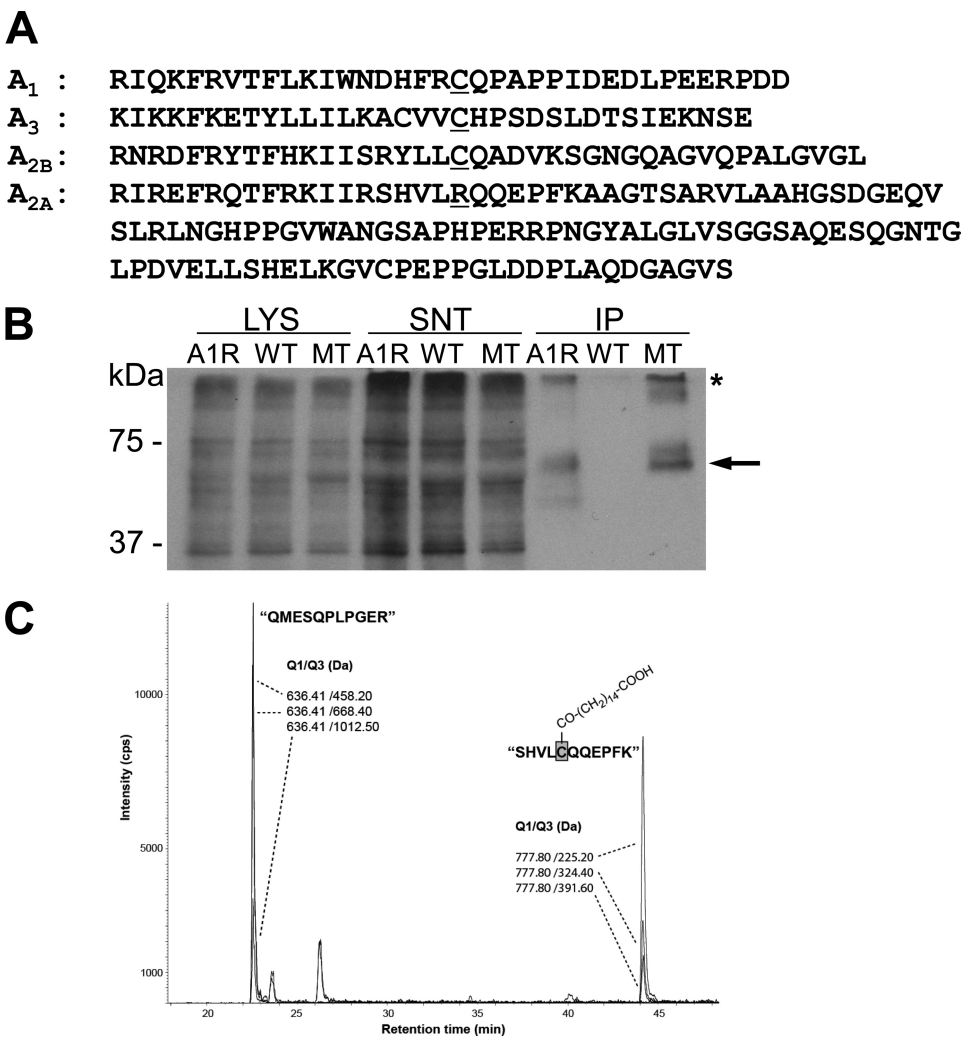

FIGURE 1. **Comparison of the C-terminal sequences of the four human adenosine receptors (*A*) and palmitoylation of the A_{2A}-R309C receptor detected by autoradiography (*B*) and by mass spectrometry (*C*).** *A*, the sequences of the C termini of the four human adenosine receptors are shown starting with the first residue after the seventh transmembrane helix. The cysteine residue that is the (putative) palmitoylation site is *underlined*; it is present in the A_1, A_3, and A_{2B} receptors but not in the A_{2A} receptor, which has an arginine residue (Arg-309) in this position. It is also evident that the C terminus of the A_{2A} receptor is substantially longer than that of any of the other receptors. *B*, HEK293 cells (3×10^5 cells) were transiently transfected with plasmids encoding the YFP-tagged wild type A_{2A} receptor (*lanes* labeled *WT*), A_1 receptor (*lanes* labeled *A1R*), or A_{2A}-R309C receptor mutant (*lanes* labeled *MT*) and incubated in the presence of [^{3}H]palmitate for 1 h. Thereafter, the cells were lysed, and solubilized material was immunoprecipitated with an antibody against GFP, lysates (*LYS*; 20 μg), supernatants (*SNT*, 20 μg), and immunoprecipitates (*IP*, corresponding to 2.5×10^5 cells) were electrophoretically resolved, and radioactively labeled bands were visualized by fluorography. The *arrow* indicates the position of the palmitoylated A_{2A}-R309C receptor band, and the *asterisk* indicates aggregated material. *C*, shown is mass spectrometry. An extracted ion chromatogram from the MRM experiments identify the presence of palmitoylation at the C terminus of the A_{2A}-R309C receptor. Three specific MRM Q1/Q3 transitions of the mutant tryptic peptide (*SHVLC**QQEPFK*, the *asterisk* indicates the palmitoylated cysteine) and the A_{2A} receptor internal control peptide (*QMESQPLPGER*) were monitored as outlined under "Experimental Procedures" and are indicated by *dashed lines*. The chromatogram was prepared with the Analyst 1.5.2 software using Gaussian smoothing and background subtraction.

ceptible to palmitoylation by using two independent approaches, namely metabolic labeling (Fig. 1*B*) and mass spectrometry (Fig. 1*C*). HEK293 cells were transfected with plasmids encoding either wild type, mutated A_{2A} receptor, or the A_1 receptor (as a positive control) with a FLAG epitope at the N terminus and a YFP fused to the C terminus to visualize receptor expression (see below Fig. 2). Cells were metabolically labeled with [^{3}H]palmitate, and the receptors were immunopurified from detergent lysates. As shown in Fig. 1*B*, immunoprecipitation of both the A_1 receptor (*lane IP A1R*) and the A_{2A}-R309C receptor mutant (*lane IP MT*) recovered radioactively labeled bands migrating with an apparent molecular mass of ~70 kDa (marked with an *arrow* in Fig. 1*B*). The apparent molecular mass is consistent with that expected from the sum of the receptor and the fluorescent protein. The double bands arise from the differently glycosylated forms (36). For both receptor types, aggregates were seen at the *top of the gel* (marked with an *asterisk* in Fig. 1*B*). In contrast and as expected, we did not recover any labeled band in immunoprecipitates of the wild type A_{2A} receptor consistent with the fact that this receptor is not palmitoylated (*lane IP WT* in Fig. 1*B*).

In agreement with this observation, the palmitoylation of Cys-309 of mutant A_{2A} receptor was verified by mass spectrometry. FLAG-tagged receptors (mutant and wild type) were immunopurified and digested with trypsin, and the resulting peptides were resolved by nano-LC and analyzed by tandem MS. Using this approach we identified several receptor-specific

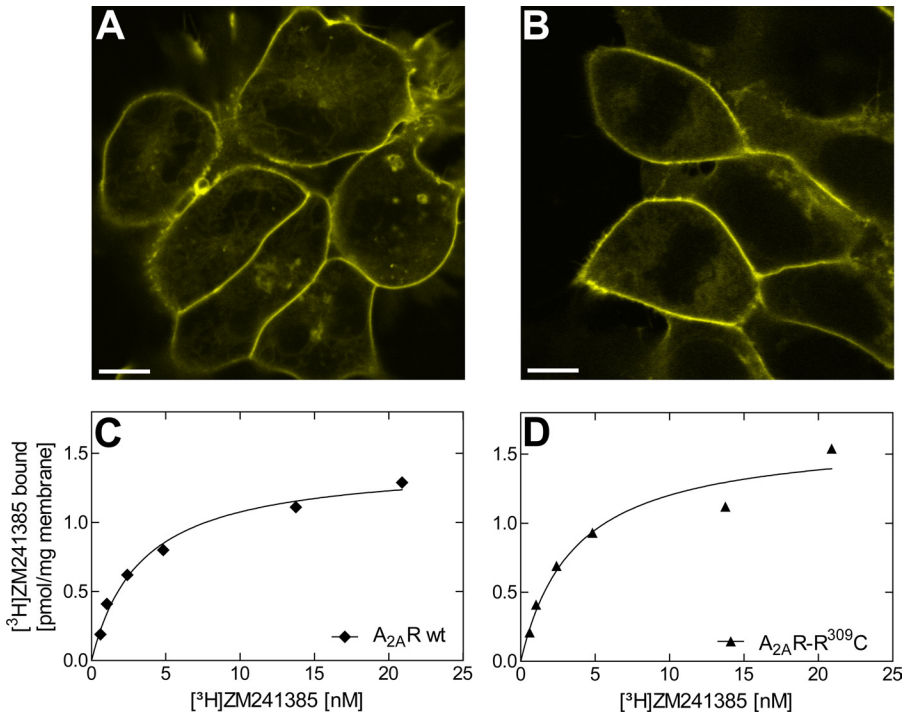

FIGURE 2. **Expression of wild type A_{2A} receptor and A_{2A}-R309C receptor in HEK293 cells.** Shown is a representative example of YFP-tagged wild type A_{2A} receptor (*A*) and A_{2A}-R309C receptor (*B*) visualized by confocal microscopy. The *bar* represents 10 μm. *C* and *D*, shown is binding of the radioligand antagonist [^{3}H]ZM241385 to membranes prepared from HEK293 cells stably expressing wild type A_{2A} receptor (*C*) and A_{2A}-R309C receptor (*D*). The membranes (5 μg/assay) were incubated with the indicated concentrations of [^{3}H]ZM241385 as outlined under "Experimental Procedures." Nonspecific binding was determined in the presence of 10 μM xanthine amino congener and was subtracted. Nonspecific binding was less than 10% in the K_D concentration range. Data are the means from duplicate determinations in a representative experiment that was reproduced three times with similar results.

peptides with a significant ProtScore (>2) and a total receptor sequence coverage of 41%. The following two peptides were used for subsequent MRM experiments to identify the thioester-linked palmitate: SHVLC*QQEPFK (the asterisk indicates the palmitoylated cysteine) and QMESQPLPGER. Fig. 1*C* shows the extracted ion chromatogram from the MRM experiments and indicates the presence of the palmitate moiety in the mutant A_{2A}-R309C receptor.

We also verified that the mutation of arginine at position 309 to cysteine did not affect folding and surface localization by visualizing the receptor (Fig. 2, *A* and *B*) and by monitoring ligand binding (Fig. 2, *C* and *D*). Both the wild type (Fig. 2*A*) and the mutated A_{2A} receptor (Fig. 2*B*) were predominantly localized at the plasma membrane of stably transfected HEK293 cells. Similarly, binding of the A_{2A} receptor antagonist [^{3}H]ZM241385 resulted in comparable saturation curves (Fig. 2, *C* and *D*) with K_D values of 3.3 ± 0.5 and 3.6 ± 1.0 nM for wild type A_{2A} receptor and the R309C mutant, respectively. In the cell clones selected, B_{max} values were similar with 1.4 ± 0.07 and 1.6 ± 0.16 pmol/mg for wild type A_{2A} receptor and A_{2A}-R309C receptor, respectively.

Accumulation of cAMP in HEK293 Cells Expressing Wild Type and Mutated A_{2A} Receptor—GPCRs, such as β-adrenergic receptors or rhodopsin, engage their cognate G protein by collision coupling. In contrast, it has long been known for the A_{2A} receptor that the rates of adenylyl cyclase activation via this receptor are incompatible with this model (21, 22). Rather, early studies revealed that the A_{2A} receptor was tightly coupled to the effector adenylyl cyclase in a manner that was accounted for by a restricted collision coupling model (20–22). Restricted collision coupling arises from the fact that the receptor can only activate a fraction of the cellular complement of its cognate G protein(s). In the case of the A_{2A} receptor, only a fraction of all available G_s is activated. This translates into a concentration-response curve in which increased receptor expression only enhances E_{max} (the maximum level of cAMP accumulation) but does not shift the EC_{50} to the left. Mechanistically, restricted collision coupling can be accounted for by a model where the cell surface membrane is compartmentalized and the receptor can only visit some of these compartments. We surmised that restricted collision coupling and the lack of palmitoylation are causally related. To test this hypothesis, several stable cell clones were obtained by selection with Geneticin; three and four clones were selected for wild type and R309C mutant receptor, respectively, based on the following criteria; (i) the level of expression was reasonably similar for wild type receptor and the R309C-mutated form, (ii) the concentration of receptor in the membrane covered a physiologically relevant range, and (iii) clones with high (*i.e.* >2 pmol/mg) expression levels were not included in the analysis. We determined cAMP accumulation after stimulation the cells with increasing concentrations of the A_{2A}-selective agonist CGS21680. As anticipated, increasing expression levels of the wild type receptor only resulted in an increase in maximum accumulation of cAMP, but the EC_{50} of the agonist was in the range of 70–80 nM irrespective of the receptor levels (Fig. 3, *A* and *C*). In contrast, increasing the expression levels of the A_{2A}-R309C receptor mutant resulted in a shift in the concentration response curve to the left (Fig. 3*B*).

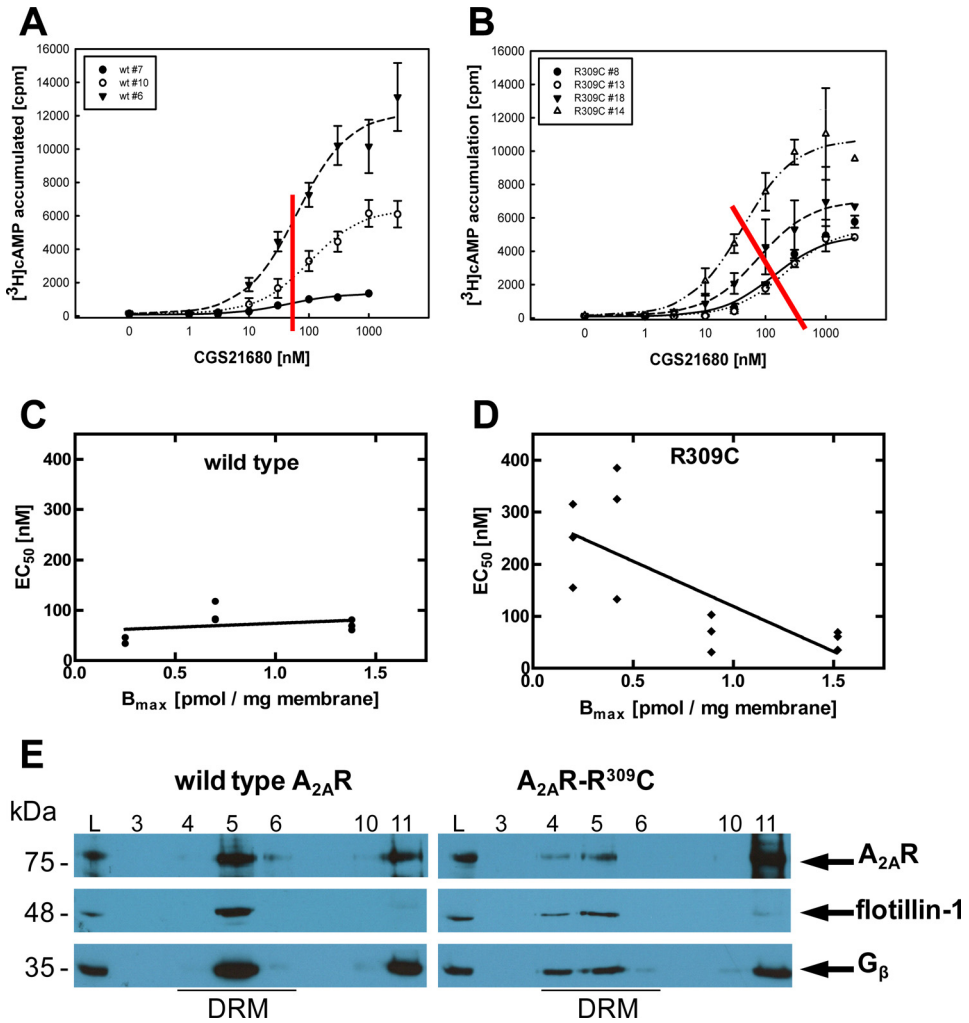

FIGURE 3. **Accumulation of [^{3}H]cAMP in HEK293 cells stably expressing wild type A_{2A} receptor (*A* and *C*) and A_{2A}-R309C receptor (*B* and *D*) at different levels and association of agonist-activated receptors with detergent-resistant membranes (*E*).** HEK293 cells were stably transfected with plasmids encoding wild type A_{2A} receptor and A_{2A}-R309C receptor and clones (wt #7, #10, #6; R309C #8, #13, #18, #14) selected. Receptor expression levels were determined in binding experiments as in Fig. 2, and the corresponding B_{max} values are plotted in *panels B* and *C*. Cells (3×10^5/well) were metabolically labeled with [^{3}H]adenine for 16 h. After the addition of fresh medium, cAMP production was stimulated by the indicated concentrations of CGS21680 for 20 min. Data are the means ± S.D. from three experiments. The *red line* in *A* and *B* connects the EC_{50} values in the individual curves. In *panels C* and *D*, EC_{50} values calculated from individual concentration-response curves are plotted as a function receptor levels (B_{max}) to illustrate the inverse correlation in cells expressing A_{2A}-R309C receptor (*D*) and the absence of any correlation in cells expressing the wild type receptor (*C*). *E*, HEK cells expressing either YFP-tagged wild type A_{2A} receptor or A_{2A}-R309C receptor were stimulated with 3 μM CGS21680 for 30 min. Membranes were prepared from these cells, extracted with 0.25% Triton X-100, and subjected to centrifugation on discontinuous sucrose gradients (by flotation). After ultracentrifugation, fractions (1 ml) were collected from the top. All fractions were analyzed; shown are fractions 3, 4, 5, 6, 10, and 11 (25 μl each) and the loaded lysate (*L*; 6 μl) that were resolved on the same denaturing polyacrylamide gel, transferred to nitrocellulose, and immunoblotted using antibodies to A_{2A} receptor, flotillin-1, and Gβ. The light fractions from the top of the gradients are on the *left*, and the heavy bottom fractions are on the *right*. The position of fractions containing detergent-resistant membranes (*DRM*) is indicated.

Accordingly, the EC_{50} was inversely related to the expression level of the mutant receptor (Fig. 3*D*). As a control, we replaced arginine in position 309 by alanine; the resulting mutant A_{2A} receptor-R309A also accumulated at the cell surface of HEK293 cells and effectively activated cAMP accumulation. In fact, the apparent agonist affinity was higher than in the wild type receptor (data not shown); however, EC_{50} values did not differ if cells expressing low and high levels of receptors were compared (2 ± 0.2 and 2.1 ± 0.3 nM, respectively). In addition, we examined the association of the agonist-activated wild type A_{2A} receptor and the mutated A_{2A}-R309C receptor with detergent-resistant membranes. Fig. 3*E* shows that in these sucrose gradients a large portion of the agonist-activated wild type receptors was retrieved in the flotillin-1-containing fractions. In contrast, the bulk of the agonist-activated A_{2A}-R309C receptor was recovered in the bottom fractions that were depleted of the raft marker flotillin-1.

Ternary Complex Formation by the A_{2A}-R309C Receptor Mutant—The substitution of arginine 309 by a cysteine residue and the resulting palmitoylation did not affect antagonist affinity (Fig. 1, *C* and *D*). However, it is evident from Fig. 3, *C* and *D*, that the EC_{50} of the agonist was increased at low expression levels of A_{2A}-R309C receptor when compared with the EC_{50} for the wild type receptor at corresponding expression levels. At high levels of expression, the difference in EC_{50} was eliminated, and EC_{50} values were virtually identical. A trivial explanation may be a drop in agonist affinity induced by the mutation. We, therefore, determined the affinity of the agonist CGS21680 in competition experiments with the radiolabeled antagonist (Fig. 4). In membrane preparations, the A_{2A} receptor is known to

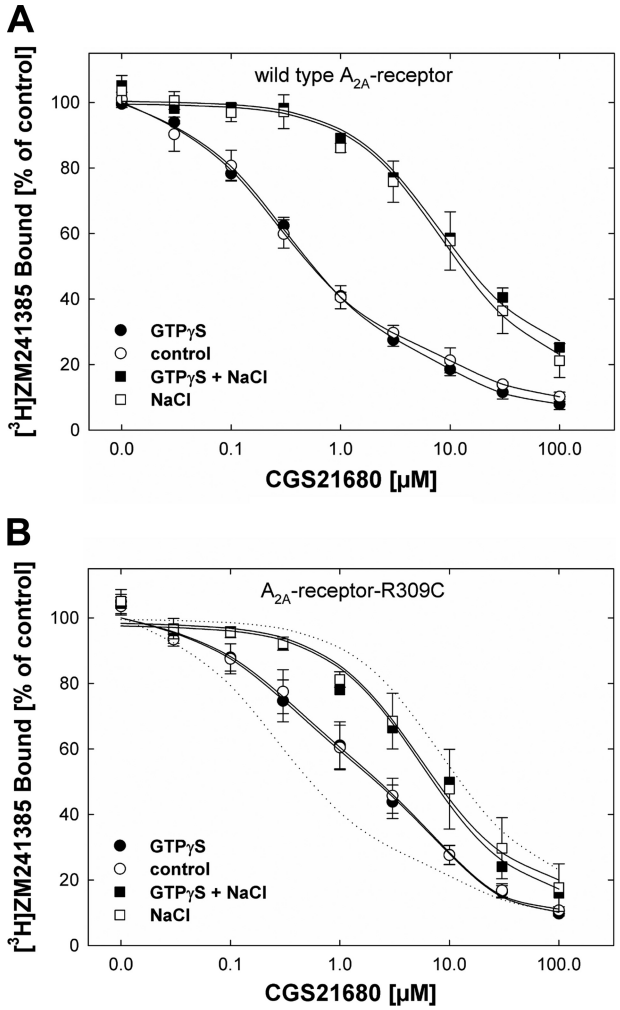

FIGURE 4. **Competition of the agonist CGS21680 for binding of the antagonist [^{3}H]ZM241385 to membranes of HEK293 cells stably expressing wild type A_{2A} receptor (*A*) and A_{2A}-R309C receptor (*B*).** Membranes (30–40 μg) prepared from HEK293 cells (clones wt #6 and R309C #14, *cf.* Fig. 3) were incubated with 3 nM [^{3}H]ZM241385 and the indicated concentrations of CGS21680 in the absence (*open circle*) or presence of 100 μM GTPγS (*filled circle*), 150 mM NaCl (*open square*) or 100 μM GTPγS and 150 mM NaCl (*filled square*). Data represent the mean ± S.E. of ≥3 independent experiments carried out in duplicate.

form high affinity agonist binding sites (reflecting the ternary complex HRG of agonist H, receptor, and G protein) that are resistant to dissociation by guanine nucleotides. The ternary complex can, however, be disrupted by the addition of NaCl (17, 37). This phenomenon is exemplified in Fig. 4*A* for the wild type A_{2A} receptor. The addition of NaCl converted the mixture of high and low affinity binding sites (ratio 3:1, Fig. 4*A*) into a homogeneous population of low affinity binding sites. In contrast, the addition GTPγS did *per se* not suffice to shift the competition curve (*filled symbols* in Fig. 4*A*). Introducing a palmitoylation site did not affect the ability of the resulting A_{2A}-R309C receptor to form GTPγS-resistant high affinity sites, but the proportion of high-affinity sites was reduced (Fig. 4*B*). By subjecting the data to curvilinear regression, the ratio of high to low affinity sites was estimated to be about 1:1. In contrast, the affinity of the agonist for the high affinity sites was comparable to that seen for the wild type receptor (K_i = 0.14 ± 0.02 and 0.18 ± 0.06 μM for wild type and mutated receptor, respectively). Upon the addition of NaCl, the competition curve was shifted to the right (*squares* in Fig. 4*B*). The shift was, however, less pronounced than that seen for the wild type receptor (*cf. dashed line* in Fig. 4*B*, which indicates the position of the corresponding competition curve for the wild type). This suggests that, in the absence of G protein coupling, the mutated receptor has a modestly enhanced affinity for the agonist (K_i = 8.6 ± 1.6 and 5.4 ± 1.1 μM for wild type and mutated receptor, respectively). This conclusion is also substantiated by the observation that the calculated affinity of CGS21680 for the low affinity site of the biphasic curve was also higher in the mutated receptor (K_i = 12.3 ± 4.1 and 4.1 ± 1.1 μM for wild type receptor and A_{2A}-R309C receptor, respectively).

Effect of Mutation on Signaling via MAPK Pathway—In endothelial cells, the A_{2A} receptor stimulates ERK/MAP kinase in a manner independent of G_s (8). This can be recapitulated in HEK293 cells (36) where stimulation of ERK does not require signaling via any G protein (26) but is contingent on recruitment of ARNO (the exchange factor for ARF6) (39). Stimulation of ERK and activation of cAMP accumulation appears to occur in physically separated membrane compartments (17). Hence, we explored whether the presence of the palmitoylation site also affected the receptor-mediated stimulation of ERK by immunoblotting for dually phosphorylated (active) ERK1 and ERK2. As previously described (see *e.g.* Ref. 17), the time course of ERK phosphorylation was biphasic and was comparable in cells expressing wild type and mutated receptor (data not shown). In cells expressing the wild type A_{2A} receptor, the concentration-response curves for the agonist CGS21680 were independent of receptor levels (*cf. panels A*, *C*, and *E* in Fig. 5) with EC_{50} values of 6.3 ± 3.4 and 9.2 ± 3.7 nM for low and high receptor levels, respectively. In contrast, in cells expressing the A_{2A}-R309C receptor, the agonist concentration-response curve was shifted to the left as receptor levels increased (*cf. panels B*, *D*, and *F* in Fig. 5) with EC_{50} values of 25.6 ± 6.7 and 6.3 ± 3.4 nM, respectively.

Determination of Receptor Mobility by Single Particle Tracking—Regardless of whether cAMP accumulation or ERK activation was examined, the agonist-activated A_{2A}-R309C receptor differed from the wild type receptor because the apparent EC_{50} depended on receptor levels. In addition, the agonist-liganded wild type A_{2A} receptor was associated to a larger extent with detergent-resistant membranes than the mutated A_{2A}-R309C receptor. We surmised that these altered properties ought to be linked to a change in receptor diffusion. We initially attempted to verify changes in receptor mobility by resorting to fluorescence recovery after photobleaching (FRAP). This approach suggested that wild type and mutant receptor differed, but in paired experiments we observed either variations in the time constant of fluorescence recovery or in the mobile fraction (data not shown, see also below). Because fluorescence recovery after photobleaching measures the properties of the receptor ensemble, these two variables are not independent. Accordingly, we labeled the receptors with quantum dots to measure the mobility of individual molecules. Two types of trajectories were observed. (i) In some instances a receptor molecule was locally confined and did not escape from this local confinement over the entire observation period, *i.e.*

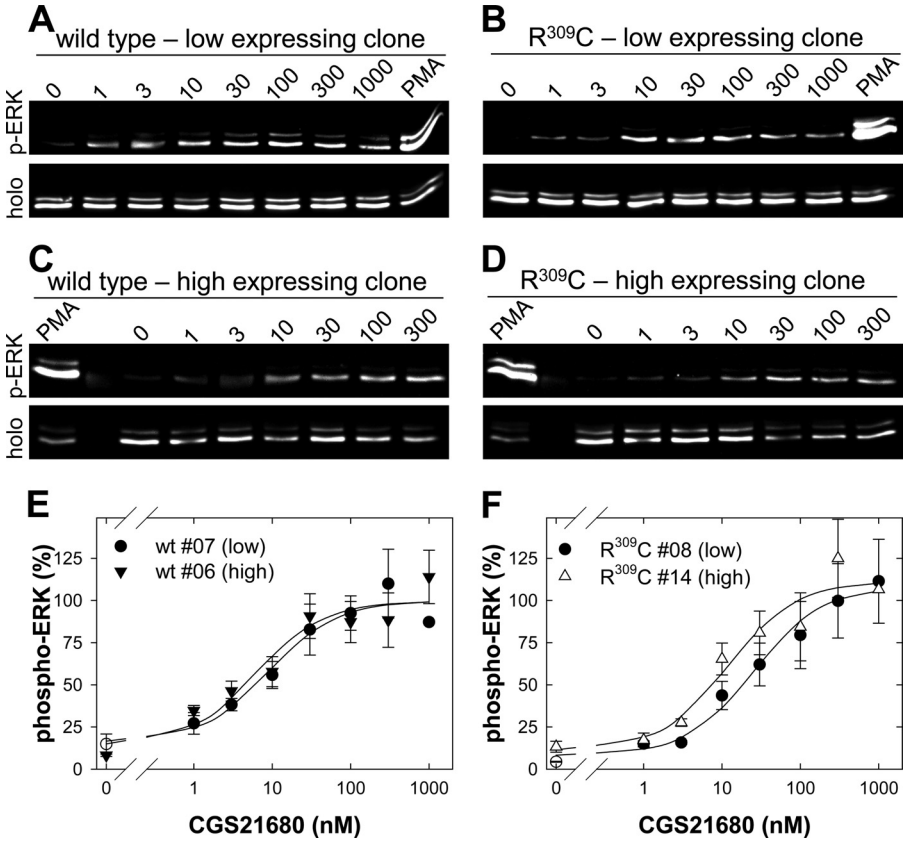

FIGURE 5. **Concentration-response curve for agonist-stimulated ERK phosphorylation in HEK293 cells stably expressing wild type A_{2A} receptor (*A*, *C*, and *E*) and A_{2A}-R309C receptor (*B*, *D*, and *F*).** Confluent serum-starved cells (3×10^5/well) expressing wild type A_{2A} receptor at low (*A*, clone wt #7, *cf.* Fig. 3) or high levels (*C*, clone wt #6) or A_{2A}-R309C receptor mutant at low (*B*, clone R309C #8) or high levels (*D*, clone R309C #14) were stimulated with the indicated nM concentrations of CGS21680 for 5 min. Stimulation by 1 μM phorbol myristate acetate (*PMA*) for 20 min served in *panels A–D* as a positive control and to allow for comparison between different blots. Aliquots of cellular lysates (20 μg) were applied to SDS-polyacrylamide gels. After electrophoretic resolution and transfer to nitrocellulose, the level of active ERK1/2 was assessed by immunoblotting with an antiserum recognizing the dually phosphorylated active enzyme (*p-ERK*) or an antiserum against holo-ERK1/2 (*holo*) (loading control). Concentration-response curves were plotted by averaging densitometric estimates from three independent experiments with low and high expressing wild type (*E*) and mutant receptor (*F*); *error bars* indicate S.E.

20 s (Fig. 6*A*). (ii) More frequently, receptors moved randomly over the cell surface resulting in trajectories consistent with a random walk over the entire observation period (Fig. 6*B*). We calculated the diffusion coefficient for each individual particle from a plot of MSD against time intervals (Δt) by limiting our analysis to the first 25% of the acquisition time (*i.e.* a minimum of 100 total frames). The random walk mode (*blue* in Fig. 6, *C* and *D*) was associated with an essentially linear dependence of area with time. In contrast, fitting the trajectory of a locally confined receptor (*red curve* in Fig. 6, *C* and *E*) allowed for extracting the radius of the apparent confinement (Fig. 6*E*). On average, the radii of the confined areas were 254 ± 112 and 187 ± 50 nm for wild type and mutant A_{2A} receptor, respectively, in the absence of CGS21680. In the presence of agonist, the radii diminished, but they were also comparable, *i.e.* 116 ± 38 and 114 ± 55 nm for wild type and mutant A_{2A} receptor, respectively. If all data were pooled and the average diffusivity was determined (*i.e.* the area covered over time), it transpired that the addition of agonist reduced the diffusion coefficient for both wild type and mutant A_{2A} receptor (*cf. dashed* and *solid lines* in Fig. 6*F*). However, the effect of the agonist was modest in the case of A_{2A}-R309C receptor (*blue lines* in Fig. 6*F*) and substantially more pronounced for the wild type receptor (*red lines* in Fig. 6*F*). The variation in diffusivity of individual receptors is more readily accessible if plotted as cumulative frequency distributions (Fig. 7, *A* and *B*). This analysis highlighted that under basal conditions, the diffusivity of wild type receptor differed to a small, albeit statistically significant extent (median $D_{1-4} = 0.14$ and 0.12 $\mu m^2/s$ for wild type receptor and for A_{2A}-R309C receptor, respectively; $p < 0.01$ by Kolmogorov-Smirnov test) (Fig. 7*A*). Agonist activation resulted in a pronounced shift in the cumulative distribution curve for the wild type receptor (*red curve* in Fig. 7*B*; median $D_{1-4} = 0.05$ $\mu m^2/s$) and only had a modest effect on A_{2A}-R309C receptor (*blue curve* in Fig. 7*B*; median $D_{1-4} = 0.10$ $\mu m^2/s$), which was nevertheless significantly different from the curve obtained in the absence of CGS21680 ($p < 0.01$ by Kolmogorov-Smirnov test). Thus wild type and mutant receptor differed substantially in their agonist-induced mobility change. This is best appreciated from the histograms shown in Figs. 7, *C–E*. Under basal conditions, a Gaussian fit allows the resolution of two populations of receptors in both the wild type (Fig. 7*C*) and the mutant receptor (Fig. 7*E*). In the presence of agonist, the proportion of slowly diffusing molecules (*orange curve* in Fig. 7*D*) increased substantially in the wild type receptor at the expense of the rapidly moving species (*cf. green lines* in Fig. 7, *C* and *D*). In contrast, agonist activation virtually eliminated the slowly moving species of A_{2A}-R309C receptor (*cf.* Fig. 7, *E* and *F*) and resulted in a

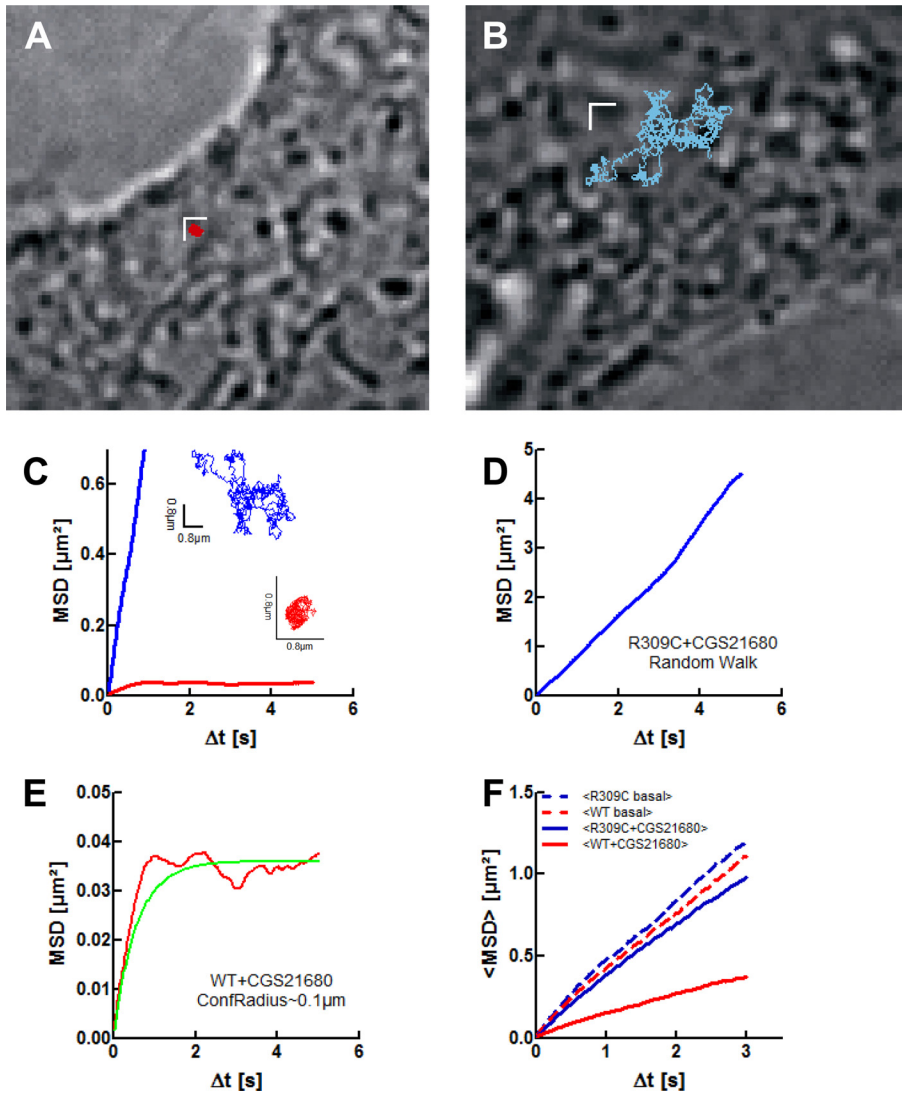

FIGURE 6. **Single particle tracking of quantum dot-labeled wild type A_{2A} receptor and A_{2A}-R309C receptor.** *A* and *B*, representative trajectories of agonist-activated wild type (*A*) and mutant receptor (*B*) were recorded as outlined under "Experimental Procedures" and projected onto the bright field image of the corresponding cell. The *scale bars* define a square of 0.8 × 0.8 μm. *C*, a MSD plot compares the trajectories for the agonist-activated wild type (*red*) and the mutant receptor (R309C, *blue*) as illustrated in *A* and *B* (and in the *insets* to *panel C*). The MSD plot was generated by fitting the data extracted from the trajectories to Equation 1 under "Experimental Procedures." Because of the large difference in MSD between the wild type and mutant A_{2A} receptor, the *y* axis was expanded in *panel D* to illustrate the random walk diffusion of the A_{2A}-R309C receptor along the illustrated blue trajectory. *E*, the confined diffusion of the wild type A_{2A} receptor was confirmed by fitting the MSD to the equation 3 describing circular confinement (see "Experimental Procedures"). The *green line* corresponds to the fitted curve. *F*, shown are averaged means square displacements of wild type (*red lines*) and mutant receptor (*blue*) recorded in the absence (*dashed lines*, basal) and presence of the agonist CGS21680 (10 μM, *solid lines*). These calculations are based on 733, 514, 755, and 713 recorded trajectories for wild type A_{2A} receptor in the basal and agonist-activated state and for the A_{2A}-R309C receptor in the basal and agonist-activated state, respectively.

homogenous population of rapid diffusivity (*solid line* in Fig. 7*F*). The *dashed lines* in Fig. 7*F* represent the fit to a distribution assuming the presence of two receptor populations. It is evident that the fit is not significantly improved. The changes in diffusivity were also evaluated by subjecting the data set to a statistical comparison using a Kruskal-Wallis test followed by Dunn's multiple post hoc comparisons; this confirmed that all observed diffusivities differed in statistically significant way (supplemental Fig. S1*A*). Agonist treatment also slowed diffusion of the A_{2A} receptor when assessed in hippocampal neurons transiently expressing a FLAG-tagged A_{2A} receptor; the median diffusion rates were 0.56 and 0.22 $\mu m^2/s$ in the absence and presence of agonist ($n > 250$ trajectories in each condition, $p < 0.01$).

We also extracted the diffusion mode from the trajectories to determine the proportion of receptors subject to confinement defined by Saxton and Jacobson (33) (see "Experimental Procedures"). In the inactive state, wild type and mutant receptor did not differ, with 0.82 and 1.46%, respectively, of the molecules displaying highly restricted macroscopic mobility (Fig. 8*A*). Agonist activation did not affect confinement of the A_{2A}-R309C receptor. In contrast, upon agonist activation, 19% of the wild type A_{2A} receptors became immobile (Fig. 8*B*). This difference was statistically significant ($p < 0.0001$, Fisher's exact test). We verified that the differences in mobility were related to the change in palmitoylation by pretreating cells expressing the wild type A_{2A} recep-

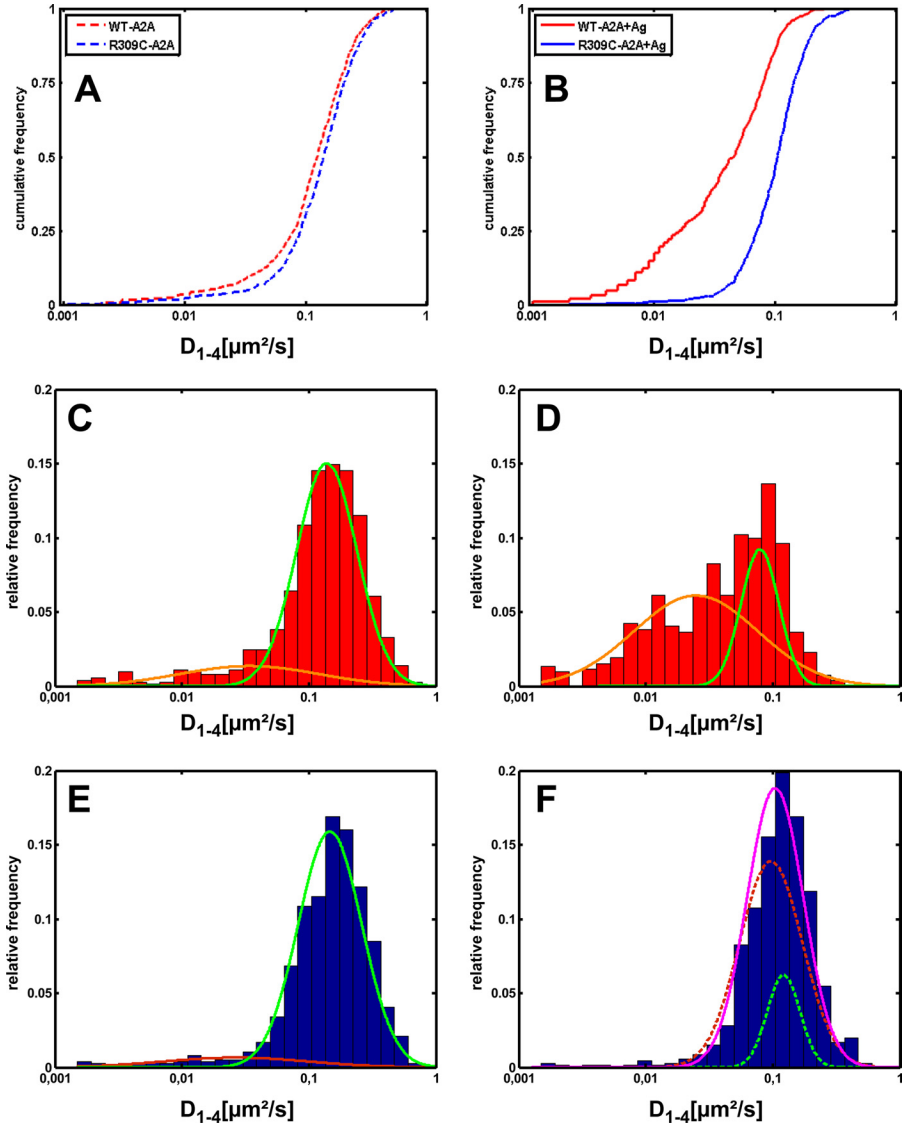

FIGURE 7. **Cumulative frequency distributions (*A* and *B*) and normalized histograms (*C–F*) for the diffusivity of the wild type A_{2A} receptor (*A*, *C*, and *E*) and A_{2A}-R309C receptor (*B*, *D*, and *F*).** Diffusivity was calculated from a linear fit to the mean square displacement of the first four recorded values (D_{1-4}) as outlined under "Experimental Procedures." The cumulative distribution are based on 733 and 755 for wild type A_{2A} receptor (*red lines*) and A_{2A}-R309C receptor (*blue lines*) in the basal state (*A*), respectively, and 514 and 713 recorded trajectories in the agonist (*Ag*)-activated state (*B*), respectively. All distributions differ in a statistically significant manner (Kolmogorov-Smirnov test, in all instances $p < 0.01$). In *panels C–F*, the data were plotted as histograms to highlight the different effect of agonist activation on diffusivity of wild type (*cf. C* and *D*) and mutant receptor (*cf. E* and *F*). The lines represent the fit assuming the presence of two Gaussian distributions. In *panel F*, the full line (*magenta*) is the fit assuming the presence of a single Gaussian distribution, whereas the *dotted lines* (*orange* and *green*) resolve two populations (without significantly improving the fit).

tor and the A_{2A}-R309C receptor with bromopalmitate, an inhibitor of palmitoylation. This pretreatment was predicted to eliminate the differences in mobility, *i.e.* the average diffusivity of agonist-activated A_{2A}-R309C receptor ought to approach that of the wild type A_{2A} receptor, if the difference was due to the presence and absence of the palmitoyl moiety. This was the case (Fig. 9*A*). The effect of bromopalmitate is most readily evident if the cumulative frequency distribution is examined (Fig. 9*B*); the cumulative distribution curve of the agonist-activated mutant receptor approached that observed for the stimulated wild type receptor (*cf.* also Fig. 9*B* and Fig. 7*B*). In fact, despite an adequate power (with >440 recordings under each condition), we failed to detect any statistically significant differences in the distributions.

DISCUSSION

In an isotropic membrane a receptor is predicted to move freely and to engage its cognate G proteins by random collision. Thus, restricted collision coupling requires anisotropy; there must be areas of the membranes that cannot readily be visited by the activated receptor, resulting in segregation of the receptor from the total available pool of its cognate G protein. We show here that for the A_{2A} receptor this is indeed the case. The wild type A_{2A} receptor controls at last two signaling cascades (11), *i.e.* the G_s-dependent activation of adenylyl cyclase and the less well defined (G_s-independent) stimulation of ERK1/2, which relies on recruitment of ARNO to the C terminus of the receptor (39) and on activation of RAS (8, 38). For both, agonist-induced cAMP accumulation and ERK phosphorylation,

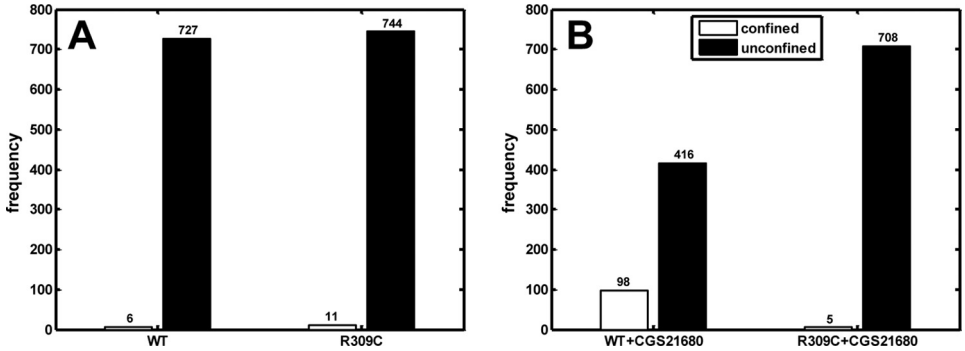

FIGURE 8. **Diffusion modes of the wild type A_{2A} receptor and the A_{2A}-R309C receptor in the absence (*A*) and presence of the agonist CGS21680 (*B*).** Trajectories were screened for the presence of events indicative of confinement as illustrated in Fig. 6*E*. The *empty bars* represent the number of trajectories that show incontrovertible evidence for confinement (see Equation 3 under "Experimental Procedures"). The difference between the wild type receptor in the basal (inactive) and the agonist-activated state is statistically significant ($p < 0.0001$, Fisher's exact test), whereas this is not the case for the A_{2A}-R309C receptor.

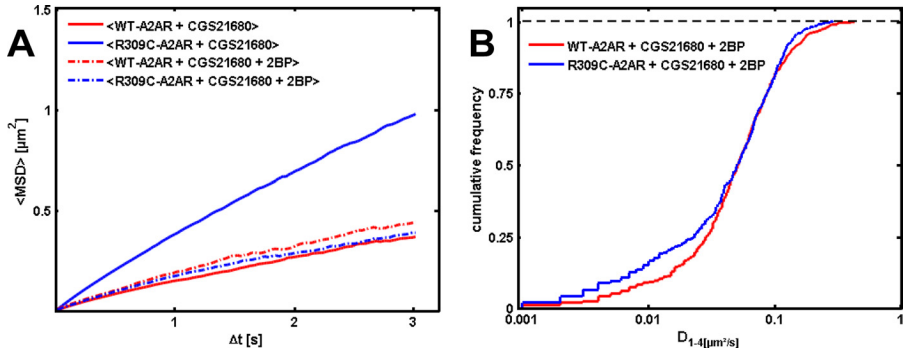

FIGURE 9. **Averaged MSD (*A*) and cumulative frequency distributions (*B*) of agonist-activated wild type A_{2A} receptor and of A_{2A}-R309C receptor in cells subjected to a pretreatment with 2-bromopalmitate.** HEK293 cells stably expressing wild type A_{2A} receptor and A_{2A}-R309C receptor were pretreated with 100 μM 2-bromopalmitate (*2BP*, *dashed lines*) for 48 h. Control cells were maintained in medium (*solid lines*). Thereafter cells were stimulated with 10 μM CGS21680; trajectories of quantum dot-labeled receptors were recorded, and averaged mean displacements (*panel A*) and cumulative frequency distributions (*panel B*) were calculated as outlined in the legends to Fig. 6 and Fig. 7, respectively. The cumulative frequency distributions are based on 445 (wt-A_{2A} receptor, *red line*) and 461 (A_{2A}-R309C receptor, *blue line*) initial D_{1-4} diffusion coefficients, and they were compared by a Kolmogorov-Smirnov test, which did not reveal any statistically significant difference ($p > 0.05$).

the EC_{50} was independent of the expression level of the A_{2A} receptor. This hallmark of restricted collision coupling was eliminated by introducing the palmitoylation site into the C terminus of the A_{2A} receptor irrespective of which pathway was examined. In addition, palmitoylation had a pronounced effect on receptor mobility, in particular in the agonist-bound state. The following arguments support the conclusion that the switch from restricted collision coupling to unrestricted collision coupling is the result of the observed changes in diffusion mode and in diffusibility. (i) Restricted collision coupling is contingent on confinement of the receptor. We observed a large increase in confinement upon agonist binding to the wild type receptor. This, however, was not seen if a palmitoylation site was engineered into the C terminus. We stress that our definition of confinement was conservative by focusing only those trajectories that were adequately described by Equation 3. Temporary confinements were not considered. (ii) In addition, in the presence of agonist we observed a pronounced redistribution of wild type A_{2A} receptors from the fast mobile pool to a slowly diffusing population. This redistribution was absent in the palmitoylated pool. By definition, in a slowly diffusing receptor species, the number of productive encounters with its cognate G protein (or any other signaling moiety) must be lower than in a rapidly moving receptor.

The number of high affinity ternary complexes observed with the palmitoylated version of the A_{2A} receptor was modestly reduced. This can be rationalized by assuming that, because of its enhanced mobility, the palmitoylated version of the A_{2A} receptor is more likely to be separated from G_s in broken cell preparations. Accordingly, a physical separation of receptors from G proteins is more probable, and the likelihood increases that the receptor will be trapped in a vesicle that does not contain any G_s. Alternative explanations, *i.e.* a reduced affinity of the receptor for the agonist or the G protein, cannot account for the decrease in ternary complexes formed by the palmitoylated version of A_{2A} receptor; in the uncoupled state, we observed a modestly increased affinity of the palmitoylated receptor for the agonist. This can be explained by assuming that the agonist-liganded structure is stabilized by membrane anchoring of helix 8 via the palmitoyl moiety. Alternatively, there may be an effect that results from the loss of the positive charge provided by the side chain of arginine 309. Similar to the wild type receptor, the palmitoylated receptor formed a tight GTPγS-resistant complex. In this ternary complex, agonist affinity was comparable in the wild type and palmitoylated receptor. We, therefore, conclude that the presence or absence of palmitoylation does not affect G protein coupling. Several earlier observations support this conclusion. Mutation of the

palmitoylated cysteine to alanine does not affect G protein-coupling of the A_1-adenosine receptor (35). This is consistent with the observation that the human A_1-adenosine expressed in *Escherichia coli*, which does not support palmitoylation, interacts with G protein with the same affinity as the receptor in brain membranes (40). We note that in several instances palmitoylation has been reported to be essential for G protein coupling; however, because these assays are based on indirect readouts of G protein-coupling in cells, they are confounded by additional events, *e.g.* enhanced desensitization of the depalmitoylated receptor (for review, see Ref. 41). In fact, all GPCRs that have been expressed in *E. coli* and reconstituted in their depalmitoylated state with G proteins bind their cognate G proteins with high affinity and with the appropriate selectivity (40, 42, 43). Earlier work also suggested a rapid agonist-induced turnover of the palmitoyl-moiety in the C terminus of the β_2-adrenergic receptor, the paradigmatic G protein-coupled receptor (44). It is worth noting though that these and related experiments were done in Sf9 cells and that they pointed to a link between depalmitoylation and phosphorylation (45). However, when examined in mammalian cell lines and quantified by mass spectrometry, palmitoylation of the β_2-adrenergic receptor was remarkably stable; there were no appreciable changes in palmitoylation up to 30 min after agonist treatment (46). After pretreatment with bromopalmitate, an inhibitor of palmitoylation, we observed a pronounced change in the diffusion of the agonist-activated A_{2A}-R309C receptor but not of the wild type receptor. These observations provide circumstantial evidence to support the assumption that agonist treatment does not result in a marked change in the palmitoylation state of the mutated receptor.

Our experiments were designed to assess the diffusion mode and the change in diffusivity upon agonist activation of a G protein-coupled receptor by using single molecule tracking. We are not aware of any other investigation that has directly visualized the local confinement of an agonist-activated G protein-coupled receptor. Accordingly, there is only a limited data set available for comparison. Using FRAP, we previously failed to detect any change in A_{2A} receptor diffusion upon agonist binding (17). FRAP also failed to detect consistent changes when we compared the wild type A_{2A} receptor and the palmitoylated variant; in some instances, paired experiments revealed a difference in the recovery time constant in the mobile fraction or both. This variability can be attributed to the ensemble nature of the FRAP recordings, which average the large heterogeneity of receptors detected by single particle tracking. Accordingly, transient confinement events may affect recovery time constant and/or the mobile fraction depending on the relative distribution of receptors subjected to synchronized bleaching in a given membrane strip. In fact, if we arithmetically average diffusion coefficients without considering the underlying distribution, we observe a considerable overlap in the mean diffusion coefficients (supplemental Fig. S1*B*). This suggests that FRAP recordings may only be sensitive enough to detect agonist-induced changes in mobility if the agonist-induced conformational change translates into a mobility shift in the dominant population of the diffusing particles. In contrast, methods that track the mobility of individual particles provide information on the heterogeneity of the molecules.

The presence of an agonist reduced the mobility of both the wild type A_{2A} receptor and to a less pronounced extent also that of the palmitoylated version. The underlying cause is not clear. Stimulation by the agonist ought to promote the formation of a receptor-G protein complex and possibly larger complexes (termed "signalosomes") that result from the association with one or several effectors. Intuitively, this situation is expected to slow receptor movement. However, agonist binding does not uniformly slow receptor diffusion; accelerated diffusion was observed for the (G_i/G_o-coupled) 5-HT_{1A} receptor (47), but the mobility of the (G_i/G_o-coupled) D_2 receptor was slowed by agonist occupancy (17). Similarly, analysis of single particles by fluorescence correlation spectroscopy showed that the diffusivity of the (G_s-coupled) CRF1 receptor was enhanced upon agonist binding, whereas that of the related (G_s-coupled) CRF2 receptor was not affected (48). This suggests that the agonist-induced change in diffusivity is an intrinsic property of the receptor protein. CRFR1 and CRFR2 differ mainly in their hydrophobic core, *i.e.* in that region of the receptor that is subject to the viscous drag of the lipid bilayer. Similarly, the palmitoylated A_{2A}-R309C receptor diffused more rapidly in both the basal unliganded and the agonist-activated state than the wild type receptor. In fact, in the presence of agonist, the palmitoyl modification rendered the distribution more homogeneous by eliminating both the slow portion of the receptor pool and the highly mobile tail of the fast population. In the x-ray crystal structure, the shape of the agonist-liganded receptor does not differ dramatically from that of the antagonist-bound receptor (13–15). However, it is worth pointing out that these structures lack a crucial component, *i.e.* the G protein; the C terminus of the G protein α-subunit has to be accommodated in a cavity created on the intracellular side (49). The resulting change in the shape of the receptor is likely to create a hydrophobic mismatch that may augment the viscous drag. In fact, based on molecular dynamics simulations, it has been argued that in the unliganded state the ligand binding pocket of the A_{2A} receptor may be invaded by phospholipid headgroups that pry apart transmembrane helix 1 and helix 2; cholesterol eliminates the hydrophobic mismatch and stabilizes the structure (16). It is conceivable that the presence of the palmitoyl moiety also exerts a stabilizing effect on the helices and thus obviates the requirement for a cholesterol-rich environment. This speculative interpretation is also consistent with the observation that the agonist-activated wild type A_{2A} receptor was more likely to visit confined areas than the version of the receptor engineered to be palmitoylated. The calculated size of the confinement area is consistent with the size of a hypothetical lipid raft. The absence of the palmitoylated A_{2A}-R309C receptor in confined areas is counterintuitive, for palmitoylation is generally thought to promote confinement in lipid rafts (41). However, a systematic proteomic survey of raft and non-raft membranes shows that *S*-palmitoylation does not represent an obligatory signal for raft association (50). In fact, there is at least one example where palmitoylation prevents a protein (*i.e.* the isoform-1 of the endothelial membrane protein TEM8) from entering lipid rafts, whereas mutation of the acceptor cysteines removes this

constraint and allows for entry into rafts (51). Thus, the most parsimonious explanation of restricted collision coupling is to attribute it to a local confinement of the A_{2A} receptor in a structure corresponding to a (putative) lipid raft.

Acknowledgments—We thank Christoph Oesterreicher and Eva-Maria Putz for providing pBABEpuro and for help in retrovirus production. Mass spectrometry data of this research have been obtained by access to the MS core facility of the Center for Physiology and Pharmacology (Medical University of Vienna).

REFERENCES

1. Fredholm, B. B. (2010) Adenosine receptors as drug targets. *Exp. Cell Res.* **316,** 1284–1288
2. Liu, R., Guo, X., Park, Y., Huang, X., Sinha, R., Freedman, N. D., Hollenbeck, A. R., Blair, A., and Chen, H. (2012) Caffeine intake, smoking, and risk of Parkinson disease in men and women. *Am. J. Epidemiol.* **175,** 1200–1207
3. Hauser, R. A., Shulman, L. M., Trugman, J. M., Roberts, J. W., Mori, A., Ballerini, R., and Sussman, N. M. (2008) Study of istradefylline in patients with Parkinson's disease on levodopa with motor fluctuations. *Mov. Disord.* **23,** 2177–2185
4. LeWitt, P. A., Guttman, M., Tetrud, J. W., Tuite, P. J., Mori, A., Chaikin, P., and Sussman, N. M. (2008) Adenosine A2A receptor antagonist istradefylline (KW-6002) reduces "off" time in Parkinson's disease. A double-blind, randomized, multicenter clinical trial (6002-US-005). *Ann. Neurol.* **63,** 295–302
5. Mantell, S., Jones, R., and Trevethick, M. (2010) Design and application of locally delivered agonists of the adenosine A_{2A} receptor. *Expert Rev. Clin. Pharmacol.* **3,** 55–72
6. Valls, M. D., Cronstein, B. N., and Montesinos, M. C. (2009) Adenosine receptor agonists for promotion of dermal wound healing. *Biochem. Pharmacol.* **77,** 1117–1124
7. Sexl, V., Mancusi, G., Baumgartner-Parzer, S., Schütz, W., and Freissmuth, M. (1995) Stimulation of human umbilical vein endothelial cell proliferation by A_2-adenosine and β_2-adrenoceptors. *Br. J. Pharmacol.* **114,** 1577–1586
8. Sexl, V., Mancusi, G., Höller, C., Gloria-Maercker, E., Schütz, W., and Freissmuth, M. (1997) Stimulation of the mitogen-activated protein kinase via the A_{2A}-adenosine receptor in primary human endothelial cells. *J. Biol. Chem.* **272,** 5792–5799
9. Palmer, T. M., and Trevethick, M. A. (2008) Suppression of inflammatory and immune responses by the A(2A) adenosine receptor. An introduction. *Br. J. Pharmacol.* **153,** S27–S34
10. Keuerleber, S., Gsandtner, I., and Freissmuth, M. (2011) From cradle to twilight. The carboxyl terminus directs the fate of the A_{2A}-adenosine receptor. *Biochim. Biophys. Acta* **1808,** 1350–1357
11. Gsandtner, I., and Freissmuth, M. (2006) A tail of two signals. The C terminus of the A_{2A}-adenosine receptor recruits alternative signaling pathways. *Mol. Pharmacol.* **70,** 447–449
12. Zezula, J., and Freissmuth, M. (2008) The A_{2A}-adenosine receptor: a GPCR with unique features? *Br. J. Pharmacol.* **153,** S184–S190
13. Jaakola, V. P., Griffith, M. T., Hanson, M. A., Cherezov, V., Chien, E. Y., Lane, J. R., Ijzerman, A. P., and Stevens, R. C. (2008) The 2.6 angstrom crystal structure of a human A_{2A} adenosine receptor bound to an antagonist. *Science* **322,** 1211–1217
14. Xu, F., Wu, H., Katritch, V., Han, G. W., Jacobson, K. A., Gao, Z. G., Cherezov, V., and Stevens, R. C. (2011) Structure of an agonist-bound human A_{2A} adenosine receptor. *Science* **332,** 322–327
15. Lebon, G., Warne, T., and Tate, C. G. (2012) Agonist-bound structures of G protein-coupled receptors. *Curr. Opin. Struct. Biol.* **22,** 482–490
16. Lyman, E., Higgs, C., Kim, B., Lupyan, D., Shelley, J. C., Farid, R., and Voth, G. A. (2009) A role for a specific cholesterol interaction in stabilizing the Apo configuration of the human A_{2A} adenosine receptor. *Structure* **17,** 1660–1668
17. Charalambous, C., Gsandtner, I., Keuerleber, S., Milan-Lobo, L., Kudlacek, O., Freissmuth, M., and Zezula, J. (2008) Restricted collision coupling of the A_{2A} receptor revisited. Evidence for physical separation of two signaling cascades. *J. Biol. Chem.* **283,** 9276–9288
18. Qanbar, R., and Bouvier, M. (2003) Role of palmitoylation/depalmitoylation reactions in G-protein-coupled receptor function. *Pharmacol. Ther.* **97,** 1–33
19. Wu, B., Chien, E. Y., Mol, C. D., Fenalti, G., Liu, W., Katritch, V., Abagyan, R., Brooun, A., Wells, P., Bi, F. C., Hamel, D. J., Kuhn, P., Handel, T. M., Cherezov, V., and Stevens, R. C. (2010) Structures of the CXCR4 chemokine GPCR with small-molecule and cyclic peptide antagonists. *Science* **330,** 1066–1071
20. Tolkovsky, A. M., and Levitzki, A. (1978) Coupling of a single adenylate cyclase to two receptors. Adenosine and catecholamine. *Biochemistry* **17,** 3811–3817
21. Braun, S., and Levitzki, A. (1979) Adenosine receptor permanently coupled to turkey erythrocyte adenylate cyclase. *Biochemistry* **18,** 2134–2138
22. Gross, W., and Lohse, M. J. (1991) Mechanism of activation of A_2 adenosine receptors. II. A restricted collision-coupling model of receptor-effector interaction. *Mol. Pharmacol.* **39,** 524–530
23. Hohenegger, M., Mitterauer, T., Voss, T., Nanoff, C., and Freissmuth, M. (1996) Thiophosphorylation of the G protein β subunit in human platelet membranes. Evidence against a direct phosphate transfer reaction to Gα subunits. *Mol. Pharmacol.* **49,** 73–80
24. Málaga-Diéguez, L., Yang, Q., Bauer, J., Pankevych, H., Freissmuth, M., and Nanoff, C. (2010) Pharmacochaperoning of the A_1 adenosine receptor is contingent on the endoplasmic reticulum. *Mol. Pharmacol.* **77,** 940–952
25. Kudlacek, O., Mitterauer, T., Nanoff, C., Hohenegger, M., Tang, W. J., Freissmuth, M., and Kleuss, C. (2001) Inhibition of adenylyl and guanylyl cyclase isoforms by the antiviral drug foscarnet. *J. Biol. Chem.* **276,** 3010–3016
26. Klinger, M., Kudlacek, O., Seidel, M. G., Freissmuth, M., and Sexl, V. (2002) MAP kinase stimulation by cAMP does not require RAP1 but SRC family kinases. *J. Biol. Chem.* **277,** 32490–32497
27. Fukata, Y., Iwanaga, T., and Fukata, M. (2006) Systematic screening for palmitoyl transferase activity of the DHHC protein family in mammalian cells. *Methods* **40,** 177–182
28. Schuck, S., Honsho, M., Ekroos, K., Shevchenko, A., and Simons, K. (2003) Resistance of cell membranes to different detergents. *Proc. Natl. Acad. Sci. U.S.A.* **100,** 5795–5800
29. Ehrensperger, M. V., Hanus, C., Vannier, C., Triller, A., and Dahan, M. (2007) Multiple association states between glycine receptors and gephyrin identified by SPT analysis. *Biophys. J.* **92,** 3706–3718
30. Mortensen, K. I., Churchman, L. S., Spudich, J. A., and Flyvbjerg, H. (2010) Optimized localization analysis for single-molecule tracking and super-resolution microscopy. *Nat. Methods* **7,** 377–381
31. Kusumi, A., Sako, Y., and Yamamoto, M. (1993) Confined lateral diffusion of membrane receptors as studied by single particle tracking (nanovid microscopy). Effects of calcium-induced differentiation in cultured epithelial cells. *Biophys. J.* **65,** 2021–2040
32. Martin, D. S., Forstner, M. B., and Käs, J. A. (2002) Apparent subdiffusion inherent to single particle tracking. *Biophys. J.* **83,** 2109–2117
33. Saxton, M. J., and Jacobson, K. (1997) Single-particle tracking. Applications to membrane dynamics. *Annu. Rev. Biophys. Biomol. Struct.* **26,** 373–399
34. Saxton, M. J. (1993) Lateral diffusion in an archipelago. Single-particle diffusion. *Biophys. J.* **64,** 1766–1780
35. Gao, Z., Ni, Y., Szabo, G., and Linden, J. (1999) Palmitoylation of the recombinant human A_1 adenosine receptor. Enhanced proteolysis of palmitoylation-deficient mutant receptors. *Biochem. J.* **342,** 387–395
36. Pankevych, H., Korkhov, V., Freissmuth, M., and Nanoff, C. (2003) Truncation of the A1 adenosine receptor reveals distinct roles of the membrane-proximal carboxyl terminus in receptor folding and G protein coupling. *J. Biol. Chem.* **278,** 30283–30293
37. Nanoff, C., Jacobson, K. A., and Stiles, G. L. (1991) The A_2 adenosine receptor. Guanine nucleotide modulation of agonist binding is enhanced by proteolysis. *Mol. Pharmacol.* **39,** 130–135

38. Seidel, M. G., Klinger, M., Freissmuth, M., and Höller, C. (1999) Activation of mitogen-activated protein kinase by the A_{2A}-adenosine receptor via a rap1-dependent and via a p21(ras)-dependent pathway. *J. Biol. Chem.* **274,** 25833–25841
39. Gsandtner, I., Charalambous, C., Stefan, E., Ogris, E., Freissmuth, M., and Zezula, J. (2005) Heterotrimeric G protein-independent signaling of a G protein-coupled receptor. Direct binding of ARNO/cytohesin-2 to the carboxyl terminus of the A_{2A}-adenosine receptor is necessary for sustained activation of the ERK/MAP kinase pathway. *J. Biol. Chem.* **280,** 31898–31905
40. Jockers, R., Linder, M. E., Hohenegger, M., Nanoff, C., Bertin, B., Strosberg, A. D., Marullo, S., and Freissmuth, M. (1994) Species difference in the G protein selectivity of the human and bovine A_1-adenosine receptor. *J. Biol. Chem.* **269,** 32077–32084
41. Chini, B., and Parenti, M. (2009) G-protein-coupled receptors, cholesterol and palmitoylation. Facts about fats. *J. Mol. Endocrinol.* **42,** 371–379
42. Freissmuth, M., Selzer, E., Marullo, S., Schütz, W., and Strosberg, A. D. (1991) Expression of two human β-adrenergic receptors in *Escherichia coli*. Functional interaction with two forms of the stimulatory G protein. *Proc. Natl. Acad. Sci. U.S.A.* **88,** 8548–8552
43. Bertin, B., Freissmuth, M., Breyer, R. M., Schütz, W., Strosberg, A. D., and Marullo, S. (1992) Functional expression of the human serotonin 5-HT1A receptor in *Escherichia coli*. Ligand binding properties and interaction with recombinant G protein α-subunits. *J. Biol. Chem.* **267,** 8200–8206
44. Loisel, T. P., Ansanay, H., Adam, L., Marullo, S., Seifert, R., Lagacé, M., and Bouvier, M. (1999) Activation of the β_2-adrenergic receptor-Gα_s complex leads to rapid depalmitoylation and inhibition of repalmitoylation of both the receptor and Gα_s. *J. Biol. Chem.* **274,** 31014–31019
45. Loisel, T. P., Adam, L., Hebert, T. E., and Bouvier, M. (1996) Agonist stimulation increases the turnover rate of β_2AR-bound palmitate and promotes receptor depalmitoylation. *Biochemistry* **35,** 15923–15932
46. Trester-Zedlitz, M., Burlingame, A., Kobilka, B., and von Zastrow, M. (2005) Mass spectrometric analysis of agonist effects on posttranslational modifications of the β_2 adrenoceptor in mammalian cells. *Biochemistry* **44,** 6133–6143
47. Pucadyil, T. J., Kalipatnapu, S., Harikumar, K. G., Rangaraj, N., Karnik, S. S., and Chattopadhyay, A. (2004) G-protein-dependent cell surface dynamics of the human serotonin 1A receptor tagged to yellow fluorescent protein. *Biochemistry* **43,** 15852–15862
48. Milan-Lobo, L., Gsandtner, I., Gaubitzer, E., Rünzler, D., Buchmayer, F., Köhler, G., Bonci, A., Freissmuth, M., and Sitte, H. H. (2009) Subtype-specific differences in corticotropin-releasing factor receptor complexes detected by fluorescence spectroscopy. *Mol. Pharmacol.* **76,** 1196–1210
49. Rasmussen, S. G., DeVree, B. T., Zou, Y., Kruse, A. C., Chung, K. Y., Kobilka, T. S., Thian, F. S., Chae, P. S., Pardon, E., Calinski, D., Mathiesen, J. M., Shah, S. T., Lyons, J. A., Caffrey, M., Gellman, S. H., Steyaert, J., Skiniotis, G., Weis, W. I., Sunahara, R. K., and Kobilka, B. K. (2011) Crystal structure of the β_2 adrenergic receptor-G_s protein complex. *Nature* **477,** 549–555
50. Yang, W., Di Vizio, D., Kirchner, M., Steen, H., and Freeman, M. R. (2010) Proteome scale characterization of human S-acylated proteins in lipid raft-enriched and non-raft membranes. *Mol. Cell. Proteomics* **9,** 54–70
51. Abrami, L., Leppla, S. H., and van der Goot, F. G. (2006) Receptor palmitoylation and ubiquitination regulate anthrax toxin endocytosis. *J. Cell Biol.* **172,** 309–320